

Multiple Filamentation of Terawatt Laser Pulses in Air

L. Bergé,¹ S. Skupin,^{1,2} F. Lederer,² G. Méjean,³ J. Yu,³ J. Kasparian,³ E. Salmon,³ J. P. Wolf,³ M. Rodriguez,⁴ L. Wöste,⁴
R. Bourayou,² and R. Sauerbrey²

¹*Département de Physique Théorique et Appliquée, CEA/DAM Ile de France, B.P. 12, 91680 Bruyères-le-Châtel, France*

²*Friedrich-Schiller-Universität Jena, Max-Wien-Platz 1, 07743 Jena, Germany*

³*Laboratoire de Spectrométrie Ionique et Moléculaire, Université Cl. Bernard Lyon 1, UMR-CNRS 5579, F-69622 Villeurbanne cedex, Lyon, France*

⁴*Institut für Experimentalphysik, Freie Universität Berlin, Arnimallee 14, D-14195 Berlin, Germany*

(Received 11 July 2003; published 2 June 2004)

The filamentation of femtosecond light pulses in air is numerically and experimentally investigated for beam powers reaching several TW. Beam propagation is shown to be driven by the interplay between intense, robust spikes created by the defects of the input beam and random nucleation of light cells. Evolution of the filament patterns can be qualitatively reproduced by an averaged-in-time (2D + 1)-dimensional model derived from the propagation equations for ultrashort pulses.

DOI: 10.1103/PhysRevLett.92.225002

PACS numbers: 52.38.Hb, 42.65.Tg, 42.65.Jx, 42.68.Ay

The self-guiding of femtosecond laser pulses in air is a well-known phenomenon nowadays exploited in, e.g., remote sensing techniques [1,2]. Infrared pulses with about 100 fs duration indeed produce narrow light filaments over long distances, along which self-phase modulation and ionization processes promote white-light emission allowing high-altitude spectroscopy experiments [2]. Self-channeling of light follows from the early self-focusing of laser radiation, caused by the Kerr response of air and leading to a sharp increase of the beam amplitude. This growth is next arrested by the electron plasma created by photoionization of air molecules, which limits the maximum intensity in the filament to $\sim 10^{14}$ W/cm². If the peak power does not exceed a few tens of critical powers for self-focusing in air ($P_{\text{cr}} \sim 2\text{--}6$ GW at 800 nm), one or two filaments are created [3–6]. At much higher powers, many of them can be generated by modulational instability of the input beam. This mechanism produces small-scale cells with each conveying a power $P_{\text{fil}} \approx \pi^2 P_{\text{cr}}/4$ [7,8], which severely degrades the homogeneity of the focal spot.

In this regard, Mlejnek *et al.* [9] proposed, from numerical inspection of a central portion of the beam, that collapsing light cells are randomly nucleated and defocused by plasma generation over short distances (<1 m) in air. Recurrence of such events then seeds a bath of short-living spiky filaments with few-critical powers and produces an optically turbulent light guide in the medium. To our knowledge, this scenario has received no experimental confirmation so far. Besides this pioneering work, a challenging issue in this field has also been to describe the evolution of an entire cm-waisted beam filamenting along extended paths at TW power levels. Although the equations governing ultrashort pulses in the atmosphere are well established, their solution requires high-performance computer machines, whose capacities are still limited for holding the fine resolution needed to resolve accurately the numerous sharp spikes

created inside broad beams, upon propagation distances covering hundreds of meters. In particular, the numerical computation of ionization channels each exhibiting a thin size of ~ 50 μm implies that, for an input beam waist of a few cm only, the required resolution in (x, y, t) can consume several terabytes of memory for a single run. Such constraints are costly in CPU time, even by using a parallel code turning on many processors. So, it may be highly beneficial to overcome this problem by integrating an alternative model that accounts, e.g., for the spatial distortions of the pulse only.

The purpose of this Letter is to elucidate, on the basis of experiments and numerical simulations, how filaments impact on the long-distance propagation of TW pulses. First, to circumvent the above numerical obstacle, we derive a reduced 2D model achieved by averaging in time the (3D + 1)-dimensional equations for ultrashort pulses in air. This simpler model is validated over meter-range distances by comparison with 3D simulations of mm-waisted pulses. It describes soliton-like states representing short-range filaments. These structures, although emitted at random, are able to confine themselves into a limited number of clusters that drive the pulse dynamics over long distances. Second, we examine two series of experiments involving the Teramobile facility [2] that delivers TW beams with either moderate ($P_{\text{in}} = 120P_{\text{cr}}$) or high ($P_{\text{in}} = 700P_{\text{cr}}$) input powers. We compare each series with results yielded by the averaged-in-time model, which restores the principal features in the experimental patterns. High-intensity defects in the spatial distribution of the input beam generate distinct zones of filaments that persist over several tens of meters, while they can excite secondary turbulent light cells.

To start with, we consider the standard propagation model, which couples an extended nonlinear Schrödinger equation for the electric field envelope \mathcal{E} , to a Drude model for the local plasma density ρ :

$$i\partial_z \mathcal{E} + \frac{1}{2k_0} \nabla_{\perp}^2 \mathcal{E} + \frac{k_0 n_2}{2} \left(|\mathcal{E}|^2 + \tau_K^{-1} \int_{-\infty}^t e^{-(t-t')/\tau_K} |\mathcal{E}(t')|^2 dt' \right) \mathcal{E} - \frac{k''}{2} \partial_t^2 \mathcal{E} - \left(\frac{k_0}{2\rho_c} - i\frac{\sigma}{2} \right) \rho \mathcal{E} + i\frac{\beta^{(K)}}{2} |\mathcal{E}|^{2K-2} \mathcal{E} = 0, \quad (1)$$

$$\partial_t \rho = \sigma_K \rho_{\text{nt}} |\mathcal{E}|^{2K} + (\sigma/U_i) \rho |\mathcal{E}|^2. \quad (2)$$

These equations, justified in [9–11], apply to fs pulses moving in their group-velocity frame, characterized by a beam waist w_0 , half-width duration t_p , central wave number k_0 , and critical power for self-focusing $P_{\text{cr}} = \lambda_0^2/2\pi n_2 = 3.3$ GW for the laser wavelength $\lambda_0 = 800$ nm and Kerr refraction index $n_2 = 3.2 \times 10^{-19}$ cm²/W. In Eq. (1), $\nabla_{\perp}^2 \equiv \partial_x^2 + \partial_y^2$ and the Kerr response of air involves a delayed (Raman) contribution where $\tau_K = 70$ fs. $\rho_c \approx 1.8 \times 10^{21}$ cm⁻³ is the critical plasma density, and power dissipation is assured by multiphoton absorption (MPA) with coefficient $\beta^{(K)} \approx 4.25 \times 10^{-98}$ cm^{2K-3}/W^{K-1}. Plasma defocusing is mainly induced by ionization of oxygen molecules with gap potential $U_i = 12.1$ eV and neutral density $\rho_{\text{nt}} = 5.4 \times 10^{18}$ cm⁻³. Plasma formation is essentially driven by multiphoton ionization (MPI) with coefficient $\sigma_K = 2.88 \times 10^{-99}$ s⁻¹ cm^{2K}/W^K and number of photons $K = 8$. Equations (1) and (2), moreover, include avalanche ionization ($\sigma = 5.44 \times 10^{-20}$ cm⁻²) and group-velocity dispersion (GVD) with $k'' = 0.2$ fs²/cm.

We now derive a reduced model, which follows from freezing the temporal dependencies of \mathcal{E} in Eq. (1). For subpicosecond durations, avalanche ionization and related absorption are ignored. We also omit GVD whose coefficient k'' is weak and assume that MPI counterbalances Kerr focusing at a time slice $t \approx t_c(z)$, where a dominant spike with temporal extent T emerges from the pulse profile and keeps the same order of magnitude along propagation. Because there exists evidence [12] that MPI shortens pulses to 1/10 of their initial duration, we choose $T = t_p/10$. Setting $\mathcal{E}(x, y, z, t) = \psi(x, y, z) \times \chi[t, t_c(z)]$, where the function χ is modeled by the Gaussian $\chi[t, t_c(z)] = e^{-[t-t_c(z)]^2/T^2}$, we plug this ansatz into Eqs. (1) and (2) and use the expression of $\rho \approx \sqrt{\pi/(8K)} T \sigma_K \rho_{\text{nt}} |\psi|^{2K} \{\text{erf}[\sqrt{2K}(t-t_c(z))/T] + 1\}$, where $\text{erf}(x)$ denotes the error function. We next integrate Eq. (1) over the entire time domain after multiplying it by χ . The equation for ψ thus reads

$$i\partial_z \psi + \frac{1}{2k_0} \nabla_{\perp}^2 \psi + \alpha k_0 n_2 |\psi|^2 \psi - \gamma |\psi|^{2K} \psi + i\nu |\psi|^{2K-2} \psi = 0, \quad (3)$$

with $\alpha = [1/\sqrt{8} + D(t_p)/4\tau_K]$, $\nu = \beta^{(K)}/2\sqrt{K}$, and $\gamma = k_0 \sigma_K \rho_{\text{nt}} \sqrt{\pi/8KT}/2\rho_c$. Here, the function

$$D(t_p) \equiv \int_{-\infty}^{+\infty} e^{(T^2/8\tau_K^2) - (u/\tau_K) - (2u^2/T^2)} \times \left\{ \text{erf}\left(\frac{\sqrt{2}u}{T} - \frac{T}{\sqrt{8}\tau_K}\right) + 1 \right\} du \quad (4)$$

follows from averaging in time the delayed Raman response. For durations $85 \leq t_p \leq 510$ fs, $D(t_p)$ varies between $0.0868t_p$ and $0.117t_p$ while $0.39 \leq \alpha \leq 0.51$, respectively. Note that this model does not depend on the longitudinal location of the time slice $t = t_c(z)$.

For testing the reliability of Eq. (3), we first simulate with Eqs. (1) and (2) the evolution of an anisotropic N th-order super-Gaussian (SG) input pulse, $\mathcal{E}_0 = \sqrt{I_0} e^{-(x^2/w_0^2 + 2y^2/w_0^2)^N - t^2/t_p^2}$, perturbed in space and time by an isotropic 10% random amplitude noise. Figure 1(a) shows the plasma strings ($\max_t \rho \propto |\mathcal{E}|_{\text{max}}^{2K}$) produced by this pulse with the beam parameters $w_0 = 0.2$ cm, $t_p = 85$ fs, $N = 2$, and $P_{\text{in}} \approx 88P_{\text{cr}}$. Integration along the z axis is performed with a spectral code in (x, y, t) running over 128 processors and using an adaptive step in z tuned on the intensity growth. Because of their dependence over $|\mathcal{E}|^{2K}$, the plasma strings, having a size in ratio $1/\sqrt{K}$ of the filament waist, provide direct information on the beam isointensities and on the location of the filaments in the (x, y) plane. The simulation shows an early disordered emission of short-scale cells nucleated at different locations, as observed in [9]. At later distances, however, these cells self-organize into three distinct channels, which do not interact significantly and conserve their

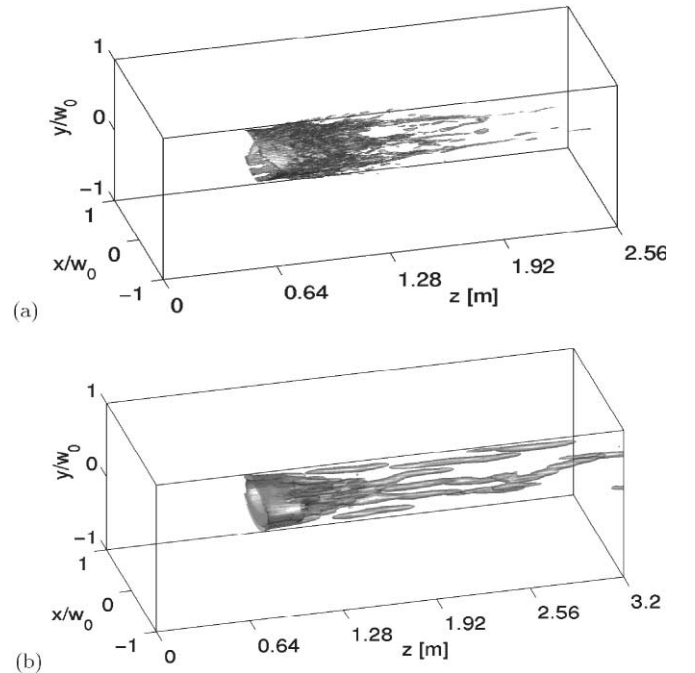


FIG. 1. (a) Plasma strings produced by a perturbed SG pulse governed by Eq. (1) with $N = 2$, $P_{\text{in}} = 88P_{\text{cr}}$, and $w_0 = 0.2$ cm. (b) Isointensity pattern of the filamentary structures created by the same pulse averaged in time following Eq. (3).

mean transverse position. For comparison, we use the fluence distribution $[\mathcal{F} = \int_{-\infty}^{+\infty} |\mathcal{E}|^2 dt]$ of the same pulse as an input datum for Eq. (3). Figure 1(b) shows the corresponding isointensity plot. Intermittency in filament nucleation occurs again in the early propagation over short ranges ≤ 0.5 m, before the filaments gather into a limited number of channels. Short-scale filaments self-attract around specific points in the diffraction plane and produce three clusters of light. These sustain a longer propagation while they still continue to excite short-living cells in their vicinity. This dynamics is qualitatively similar to that developed in Fig. 1(a).

Although restrained to a single time slice, the 2D model reproduces qualitative behaviors of the original 3D Eqs. (1) and (2). Therefore, we find it worth mentioning some major properties of the reduced equation. In the absence of MPA, Eq. (3) admits soliton solutions exhibiting an SG shape with waist w_s , $|\psi_s| \sim A_s e^{-(r/w_s)^{2N}}$, where $A_s^2 \sim (\gamma/\alpha k_0 n_2)^{1/(1-K)}$ and N decreases with the soliton power. When MPA comes into play, it is then easy to evaluate from the power conservation law the maximum dissipation range along which the power in one soliton goes below critical. This length, $\Delta z_{\text{MPA}} \approx 0.4$ m, does not depend on the beam waist and is compatible with the short “life range” of one isolated filament simulated in [9]. In contrast, when several filaments are confined in the same neighborhood, Eq. (3) predicts that they can interact and self-maintain over much longer distances (>1 m), which explains the apparent robustness of the asymptotic channels in Fig. 1.

To check this concept, we investigate some evolution stages in the filamentation patterns produced by the Teramobile laser [2]. This system delivers 10-Hz rated pulses in collimated geometry with energy up to 0.5 J, transverse diameter equal to 5 cm ($w_0 \approx 2.5$ cm), and FWHM durations ($\equiv \sqrt{2 \ln 2} t_p$) tunable from 100 to 600 fs. The coming experiments show photos taken from a white screen positioned in the plane orthogonal to the beam path. A filter with narrow bandwidth around $\lambda_0 = 800$ nm was put in front of a CCD camera.

Figure 2 details the growth of the experimental filaments (colored figures) over 55 m for pulses with 230 mJ energy and duration of 600 fs. Modulations induced by caustics in the spatial beam profile develop as follows: At the edge of the beam where fluctuations are the most intense, filaments occur along a flattened ring inside the focal spot. More filaments are then generated around this ring, which degenerates into a three-pronged fork shape before the final spreading of the beam.

For comparison, we integrated the (2D + 1)-dimensional Eq. (3) from a digitized file of the experimental input beam profile. With a pulse duration of 600 fs ($t_p \approx 510$ fs), the coefficient α in Eq. (3) takes the value $\alpha = 0.51$. Very high spatial resolution [i.e., 8192^2 points in the (x, y) plane for a box length of $6w_0$] was required, in order to solve narrow optical structures reaching $\sim 10^3$ times the input intensity I_0 . In Fig. 2, black and white

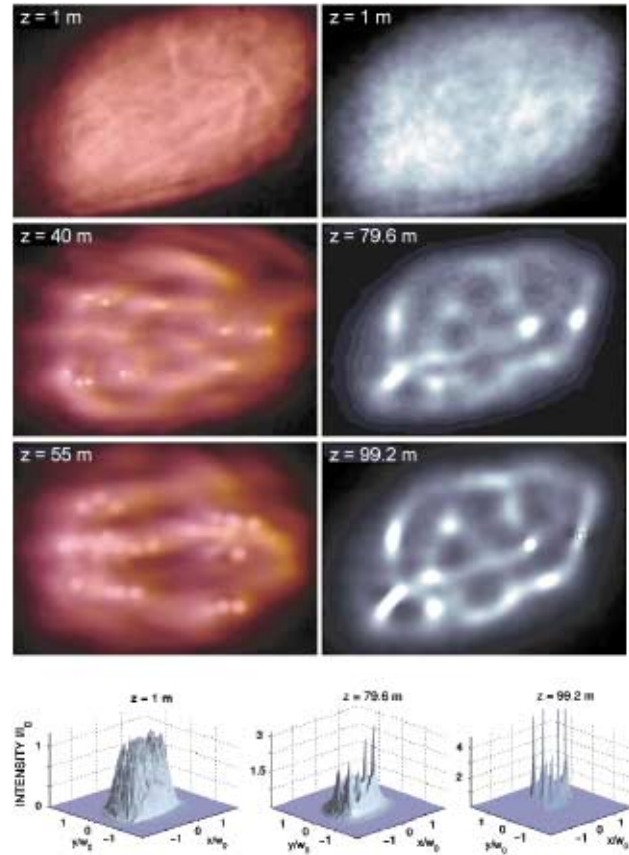


FIG. 2 (color). Left: Filamentation patterns produced experimentally for the $120P_{\text{cr}}$ beam at different propagation distances. Right: Numerical computations of the same beam from Eq. (3). Bottom row shows the major peaks forming the pattern. For clarity, the maximum intensity is limited to four times the input intensity.

figures illustrate the results of these numerical simulations. The beam containing ≈ 120 critical powers begins to form local clots from the highest intensity regions of the beam. Then, others emerge along a ring inside the lower half plane of the focal spot. The final pattern results in a trident-shaped figure, as experimentally observed. Discrepancies in the filamentation distances are attributed to our former choice $T = 0.1t_p$, which suits in the ionization regime but cannot restore the early self-focusing distances requiring rather $T = t_p$. For such beams with a few tens of critical powers only, Eq. (3) describes a disordered optical distribution having an effective power ratio of $\sim \alpha P_{\text{in}}/P_{\text{cr}} \approx 60$. This limits to 24 at the very most the number of genuine filaments reaching the ionization threshold. From these patterns, we can observe that some filamentary channels persist over several meters, whereas others are randomly nucleated over shorter longitudinal scales. The bottom row in Fig. 2 illustrates the numerically computed spatial distortions in the beam profile. These favor the growth of intense peaks that imprint the filamentation figure and locate clusters near which light cells may aggregate.

Let us notice that the resemblance between the experimental and numerical patterns does not lie, of course, in the exact position and number of the filaments, which undergo fluctuations owing to, e.g., atmospheric turbulence or local diffusive processes as they propagate. Instead, qualitative similarities occur in the following sense: Starting with an input coarse profile, the beam amplifies its initial inhomogeneities, and, through modulational instability, it produces bright spots connected by lower-intensity bridges. A “global” pattern then emerges from the zones of highest concentration of light, which form characteristic figures (ring/trident). These aspects are actually well restored by the 2D simulations, using the digitized fluence of the experimental input beam.

Figure 3 displays filamentation stages for pulses delivered by the Teramobile system, with a shorter FWHM duration of 100 fs ($t_p = 85$ fs) and 230 mJ energy. The power range here accesses 2.3 TW, i.e., about 700 critical powers. A ring-shaped zone supports major spots initiated by the highest-intense defects of the initial beam [$z \approx 30$ m]. These “hot” spots self-focus more and more over several meters, while they excite secondary smaller-scaled filaments in their vicinity [$z \approx 35$ m]. Evacuation of power excess (MPA, collapse dynamics) undergone by the primary filaments finally allows the transfer of power to the central zone of the beam, which serves as an energy reservoir for exciting new sequences of small spots [$z \approx 50$ m]. Equation (3) computed with $\alpha = 0.39$ ($t_p = 85$ fs) restores these features with less discrepancy in the filamentation distances, since the beam contains much higher power than in the previous case. From these results, we can examine specific geometrical zones in the beam pattern. Characteristic examples are indicated by the labels 1–3: (1) points to a couple of hot spots surviving at further distances; (2) indicates an active region of the beam, where intense filaments decay into cells of lesser intensity; (3) identifies an area including a cross-wise structure that keeps some filaments robust over 5 m. Spatial distortions in the 2D simulations qualitatively agree with the experimental features. The beam breaks up into more cells ($\alpha P_{in}/P_{fil} \sim 110$) than in the previous lower-power case. Note that even if some filaments are still able to survive over several meters at the most powerful regions of the pulse, random nucleation of optical cells seems here more developed than in the patterns shown in Fig. 2. At high powers, clusters of filaments cannot, indeed, propagate independently due to their smaller separation distance. They experience more substantial power transfers through the overall surface of the beam, which, therefore, increases the number of secondary cells.

In summary, we have investigated the multiple filamentation of collimated beams delivered by the Teramobile laser, for powers up to several TW. Long-range filaments are initiated by the most intense fluctuations of the input beam, and these may persist over several

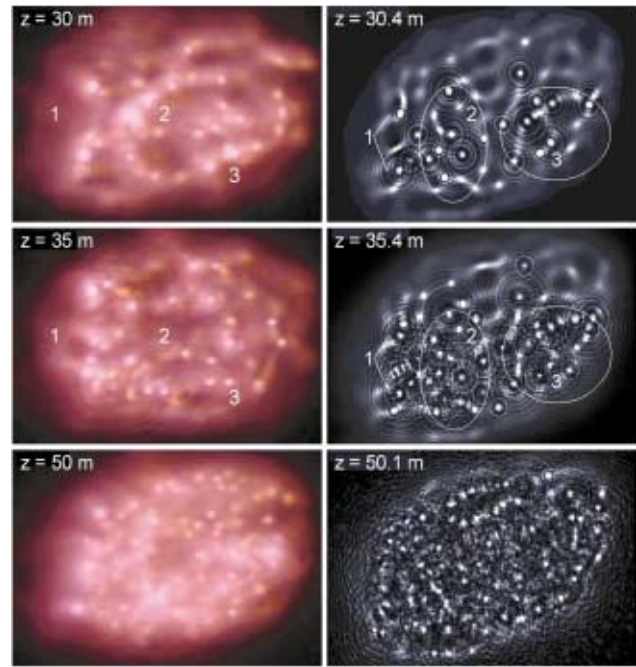


FIG. 3 (color). Left: Filamentation patterns of the $700P_{cr}$ beam delivered by the Teramobile laser. Right: Numerical computations performed with Eq. (3). Labels 1–3 spot specific beam zones commented on in the text.

tens of meters. Small-scale spots arise and recur rapidly at other places in the diffraction plane, in agreement with the scenario of “optically turbulent light guides” proposed in Ref. [9]. The long-living primary filaments, as well as unstable randomly nucleated ones, can be described by the reduced 2D model [Eq. (3)], which reproduces qualitative events in the filamentation patterns.

Experiments were realized in the framework of the Teramobile Project, funded jointly by CNRS and DFG.

-
- [1] L. Wöste *et al.*, *Laser Optoelektron.* **29**, 51 (1997).
 - [2] H. Wille *et al.*, *Eur. Phys. J. Appl. Phys.* **20**, 183 (2002); J. Kasparian *et al.*, *Science* **301**, 61 (2003).
 - [3] A. Braun *et al.*, *Opt. Lett.* **20**, 73 (1995); E. T. J. Nibbering *et al.*, *Opt. Lett.* **21**, 62 (1996); A. Brodeur *et al.*, *Opt. Lett.* **22**, 304 (1997).
 - [4] B. LaFontaine *et al.*, *Phys. Plasmas* **6**, 1615 (1999).
 - [5] S. L. Chin *et al.*, *Appl. Phys. B* **74**, 67 (2002).
 - [6] S. Tzortzakis *et al.*, *Phys. Rev. Lett.* **86**, 5470 (2001).
 - [7] V. I. Bespalov and V. I. Talanov, *JETP Lett.* **3**, 307 (1966).
 - [8] L. Bergé, Cl. Gouédard, J. Schjødt-Eriksen, and H. Ward, *Physica (Amsterdam)* **176D**, 181 (2003).
 - [9] M. Mlejnek, M. Kolesik, J. V. Moloney, and E. M. Wright, *Phys. Rev. Lett.* **83**, 2938 (1999).
 - [10] M. Mlejnek, E. M. Wright, and J. V. Moloney, *Opt. Lett.* **23**, 382 (1998).
 - [11] A. Couairon *et al.*, *J. Opt. Soc. Am. B* **19**, 1117 (2002).
 - [12] H. Ward and L. Bergé, *Phys. Rev. Lett.* **90**, 053901 (2003).